RSC Advances

PAPER

View Article Online
View Journal | View Issue

Cite this: *RSC Adv.*, 2016, **6**, 38521

SPIO@SiO_2–Re@PEG nanoparticles as magneto-optical dual probes and sensitizers for photodynamic therapy†

Marco Galli,[a] Elisa Moschini,[b] Maria Vittoria Dozzi,[a] Paolo Arosio,[ce] Monica Panigati,[aef] Laura D'Alfonso,[d] Paride Mantecca,[b] Alessandro Lascialfari,[ce] Giuseppe D'Alfonso[ae] and Daniela Maggioni*[ae]

A dual magneto-optical nanoprobe, endowed with properties useful for photodynamic therapy, has been prepared. It is constituted by a superparamagnetic iron oxide (SPIO) core (diameter size distribution centered at *ca.* 10 nm), obtained by thermal decomposition of iron oleate, coated by a compact silica shell, grown in a reverse microemulsion environment. Luminescent $[Re(phen)(CO)_3(py)]CF_3SO_3$ complexes were covalently anchored to the silica shell, by functionalizing the pyridine ligand with a triethoxysilane moiety. Finally, the surface of the nanoparticles (NPs) was coated with a layer of polyethylene glycol (PEG), functionalized with triethoxysilane, to improve stability and stealthiness in physiological conditions. Transmission electron microscopy of these SPIO@SiO_2–Re@PEG nanocomposites showed a single population, with size distribution centered at *ca.* 40 nm. NPs showed nuclear relaxivity values that guarantee an appreciable contrast in magnetic resonance imaging (r_2 > 30 s^{-1} mM^{-1} at frequencies higher than 5 MHz). The presence of the Re complexes imparted photoluminescence to the NPs, with blue shifted emission and higher photoluminescence quantum yields with respect to the free $[Re(phen)(CO)_3(py\text{-}upts)]^+$ complex (λ_{em} 553 *vs.* 580 nm, Φ 0.060 *vs.* 0.038, in aerated water solution). The complexes embedded into the NPs maintained a satisfactory efficiency toward $^1O_2$ generation (quantum yields 0.21 *vs.* 0.26 for the free complex, as assessed using 1,5-dihydroxynaphthalene as indirect marker of the $^1O_2$ presence). Preliminary cell penetration tests were performed on human lung adenocarcinoma A549 cells. Two photon excitation confocal microscopy showed that the NPs were easily internalized and accumulated in the perinuclear region of the cells already after 4 h of incubation. Increased cytotoxicity upon irradiation with respect to the dark was also observed, showing the potential of the nanocomposite for photodynamic therapy applications.

Received 17th February 2016
Accepted 11th April 2016

DOI: 10.1039/c6ra04332a

www.rsc.org/advances

1. Introduction

The use of nanoparticles (NPs) in biomedicine has attracted much attention in the past decades, for their remarkable potential in the resolution of many long-standing problems.[1] For this purpose, the NPs diameters must be in the range 10–100 nm, since smaller particles would escape from the circulatory system through renal clearance, whereas larger ones will be recognized by reticulo-endothelial system (RES), sequestered and mainly delivered to the liver. Preferential accumulation in solid tumors can be observed for NPs with size smaller than 100 nm, for the so called EPR (enhanced permeability and retention) effect, which can be further enhanced if the surface is functionalized with molecules or polymers able to make the NPs stealth to the RES.[2,3] NPs, thanks to their large surface area, can be loaded with huge amounts of small molecules, and therefore can act as efficient carriers of drugs or imaging agents toward their target, preventing their rapid clearance. In this way different diagnostic and therapeutic functionalities can be integrated in a single nanosized system. Since each imaging technique has pros and cons, nanoprobes provided with different contrast agents exploitable in different imaging techniques could provide many advantages over single monomodal probes.

[a]*Dipartimento di Chimica, Università degli Studi di Milano, Via Golgi 19, 20133 Milano, Italy. E-mail: daniela.maggioni@unimi.it*
[b]*Dipartimento di Scienze dell'Ambiente e del Territorio e di Scienze della Terra, Università degli Studi di Milano-Bicocca, Piazza della Scienza 1, 20126 Milano, Italy*
[c]*Dipartimento di Fisica, Università degli Studi di Milano, Via Celoria 16, 20133 Milano, Italy*
[d]*Dipartimento di Fisica, Università degli Studi di Milano-Bicocca, Piazza della Scienza 3, 20126 Milano, Italy*
[e]*Consorzio Interuniversitario Nazionale per la Scienza e Tecnologia dei Materiali, Via Golgi 19, 20133 Milano, Italy*
[f]*Istituto per lo Studio delle Macromolecole, Consiglio Nazionale delle Ricerche (ISMAC-CNR), Via E. Bassini, 15, 20133 Milano, Italy*

† Electronic supplementary information (ESI) available: Experimental details, DLS and TGA analyses, NMR, IR and UV-vis spectra, confocal microscope images and MTT test graphs are presented. See DOI: 10.1039/c6ra04332a

Many dual magneto-optical probes have already been reported,[4–8] in which iron oxides magnetic NPs bear light emitters, like quantum dots (QDs)[9] or organic fluorophores.[10] However the high toxicity of QDs limits their application in diagnosis, while organic fluorescent molecules often present drawbacks, such as high photobleaching, short lifetimes, and emission energy close to cell autofluorescence. The use of organometallic complexes emitting from triplet states can overcome these disadvantages, due to their generally high photostability, large Stock's shifts, which prevent self-quenching and overlapping with cell autofluorescence, and long lifetimes, which allow to improve the sensitivity by the use of time-resolved techniques. For these reasons phosphorescent metal complexes have been often proposed for imaging techniques.[11]

Among these phosphorescent emitters, diimine complexes of *fac*-$Re(CO)_3^+$ have been attracting much interest since long time, for their remarkable photophysical properties,[12] which have been exploited in a variety of fields, either for biomedical applications,[13] or material science.[14] Like other d^6 transition-metal complexes, these species exhibit an intense long-lived emission, originating from triplet metal-to-ligand charge transfer (^{3}MLCT) excited states. The strongest emissions occur either from mononuclear cationic complexes[15,16] or from dinuclear species in which two metal centers are bonded to the same chromophore.[17] The direct conjugation of a luminescent mononuclear rhenium complex "$Re(L)(CO)_3^+$" to magnetite NPs has been recently reported,[18] and this nanosystem is proposed as multimodal probe MRI T2 contrast agent, optical probe, and potential β and γ emitter through the use of $^{186/188}$Re hot isotopes, for single-photon emission tomography (γ) or radiotherapy (β).

It has been recently proven that some of these rhenium complexes are endowed with another important property for biomedical uses, *i.e.* they are efficient sensitizers for the generation of singlet oxygen,[19–23] by triplet–triplet energy transfer. Singlet oxygen production is at the base of photodynamic therapy (PDT),[24–27] which has become more and more attractive as a valid coadjuvant (or even alternative) to chemotherapy in cancer cure and as a new method for killing pathogens in localized infections.

PDT requires a photosensitizer, *i.e.* a molecule that can be photo-excited in a triplet state and is able to transfer energy to molecular oxygen, converting it from triplet to singlet state (eqn (1)).

$$^3S_1^* + {}^3O_2 \rightarrow {}^1S_0 + {}^1O_2 \quad (1)$$

Among the various species used as photosensitizers we can list organic dyes as methylene blue[28] or rose Bengal,[29] as well as porphyrins,[24] chlorines,[26,30] phthalocyanines,[24] porphycenes,[31,32] and metal complexes of Ru,[24] Ir,[33–35] Pt[36,37] and Re.[19–23] Many different nanomaterials for PDT containing transition metal complexes as photosensitizers have also recently appeared in the literature,[38–42] One only of the above nanosized systems, constituted by silica NPs, involved the use of rhenium complexes.[42]

In this work we have prepared a dual probe nanocomposite, constituted by an iron oxide magnetic core and a compact silica shell functionalized with a luminescent complex, *viz.* $[Re(phen)(CO)_3(py\text{-}upts)]CF_3SO_3$ (py-upts = 1-(pyridin-4-yl)-3-(3-(triethoxysilyl)propyl)urea). The silica shell has been coated by a polyethyleneglycol (PEG) layer. Actually, pegylation, though known to partly affect the efficiency of nanoparticles uptake, is a very effective method to reduce their toxicity.[43] Moreover, polyethylene glycols *in vitro* enhance the nanoparticles stability and *in vivo* allow the nanoparticles to avoid macrophage recognition, uptake and clearance from systemic circulation.[44] The photophysical and relaxivity properties of the SPIO@SiO_2–Re@PEG nanocomposites have been measured, to check the possible mutual interference between the magnetic core and the luminescent shell. Preliminary cell penetration tests have been conducted on human lung adenocarcinoma A549 cells to investigate the internalization of SPIO@SiO_2–Re@PEG NPs as well as the molecular probe, by means of two photon excitation (TPE) confocal microscopy. The ability of the nanocomposites to act as PDT agents has also been investigated, both in cuvette and *in vitro*.

2. Experimental

Materials, Instruments and Methods are detailed in ESI,† as well as the synthesis of the SPIO@OA NPs, of the py-upts ligand and of PEG_{500}-silane.

2.1. Synthesis of the [Re(phen)(CO)$_3$(py-upts)]OTf complex

$Re(CO)_5OTf$[45] (OTf = CF_3SO_3, 37.2 mg, 7.83×10^{-2} mmol) was dissolved in dry toluene (8 mL) under nitrogen, and added with 15.5 mg of 1,10-phenanthroline monohydrate (7.8×10^{-2} mmol). The mixture was heated at 100 °C for 5 h. Finally, the temperature was lowered to 0 °C, giving an orange powder, from which the intermediate product [Re(phen)(CO)$_3$(OTf)] was isolated by washing with toluene (3 mL, 2 times) and drying under vacuum. Yield 96%. The progress of the reaction was monitored by IR spectroscopy and the final IR spectrum showed ν(CO) bands (CH_2Cl_2) at 2035 (*vs.*), 1935 (s) and 1915 (s) cm^{-1}. The pyridine ligand py-upts (20.9 mg, 0.0644 mmol) was dissolved in 1 mL of anhydrous ethanol under nitrogen. Then, a sample of [Re(phen)(CO)$_3$(OTf)] (38.6 mg, 0.0643 mmol), dissolved in 2 mL of EtOH, was added. The initial suspension was heated at 50 °C and left to react under magnetic stirring and nitrogen for 48 h, obtaining a clear and yellow solution. In order to avoid the hydrolysis of the ethoxy groups, the resulting complex [Re(phen)(CO)$_3$(py-upts)]OTf was not isolated and was stored at 4 °C in ethanol solution under nitrogen. The completeness of the coordination of py-upts was assessed by ^{1}H-NMR. ^{1}H NMR (400 MHz, MeOD) δ 9.72 (dt, J = 5.1, 1.2 Hz, 2H), 8.95 (dt, J = 8.3, 1.2 Hz, 2H), 8.25 (s, 2H), 8.13 (dd, J = 8.3, 5.1 Hz, 2H), 8.05 (d, J = 6.0 Hz, 2H), 7.19 (d, J = 6.0 Hz, 2H), 3.79 (quart, J = 7.2 Hz, 6H), 3.11 (m, 2H), 1.53 (m, 2H), 1.18 (t, J = 7.2 Hz, 9H), 0.57 (m, 2H). FTIR ν(CO): 2034 (*vs.*), 1934 (br, s) cm^{-1} (ethanol); 2033 (*vs.*), 1924 (br, s) cm^{-1} (water).

2.2. Coating of the SPIO NPs with a SiO_2 shell

The silica coating was obtained by a synthesis conducted in a reverse microemulsion. IGEPAL CO-520 (2.7385 g, 6.21 mmol) was dissolved by sonication (20 min) in 22 mL of cyclohexane, in a Schlenk round bottom flask. Then SPIO@OA NPs (0.82 mg, see ESI†) were added, together with aqueous NH_3 (28%, 200 μL) and TEOS (150 μL, 0.677 mmol) to give a brown clear solution. The microemulsion was stirred for 16 h at room temperature, then treated with ethanol (20 mL) and centrifuged (7550 g, 20 min). The precipitate was recovered and easily re-suspended in 20 mL of ethanol by sonication. The purification procedure was repeated twice.

2.3. Functionalization of the SPIO@SiO_2 NPs with [Re(phen)$(CO)_3$(py-upts)]OTf and PEG_{500}-silane

The ethanol suspension of SPIO@SiO_2 NPs was treated with an ethanol solution of the complex [Re(phen)$(CO)_3$(py-upts)]OTf (310 μL, containing *ca.* 1 mg of complex, see ESI†) and a few drops of aqueous NH_3 (28%), as catalyst. The suspension was refluxed for 5 h, by magnetic stirring under nitrogen, then the mixture was cooled to room temperature, and treated with H_2O (4 mL), aqueous NH_3 (28%, 600 μL) and PEG_{500}-silane (60 μL, *ca.* 0.126 mmol, see ESI†). The reaction was allowed to proceed under magnetic stirring for 48 h. Then, the NPs were isolated by centrifugation (15 min at 7550 g) and finally suspended in 20 mL of milliQ water and stored at 4 °C for further uses. FTIR (water) ν(CO): 2033 (*vs.*), 1924 (br, s) cm^{-1}. The content of Fe and Re in the mother solution was determined by ICP-AES on a sample digested as follows: 1.00 mL of the NP suspension was dried on a sand bath, added with 1 mL of a 70 : 30 mixture of concentrated HCl and HF (36% and 48%, respectively), and allowed to react for 30 min under sonication in a Teflon vial at room temperature. The excess of HF was quenched by addition of H_3BO_3 (2 mmol). Then, a mixture of concentrated HNO_3 and H_2O_2 (1 : 2 ratio, 1.5 mL) was added and left to react overnight at room temperature. [Fe] from ICP-AES = 1.2×10^{-4} M (6.7 μg mL^{-1} Fe); [Re] from ICP-AES = 3.8×10^{-5} M.

2.4. Photochemical stability test on [Re(phen)$(CO)_3$(py-upts)]OTf

A sample of [Re(phen)$(CO)_3$(py-upts)]OTf was dissolved in water saturated with O_2. The solution was exposed to visible light (by using a 150 W/NDL lamp, 390 nm cutoff filter, 142 mW cm^{-2} see Fig. S1†), and UV-vis absorption spectra were recorded every 15 min for 1 h (Fig. S2†).

2.5. Singlet oxygen production

In a quartz cuvette 0.555 mL of the above described mother solution of SPIO@SiO_2–Re@PEG NPs were added to 1.70 mL of a H_2O/MeOH 80 : 20 mixture, affording a [Re] = 1×10^{-5} M. Subsequently 1,5-dihydroxynaphthalene (DHN) (0.25 mL of a MeOH solution 1×10^{-3} M) was added to give a [DHN] = 1×10^{-4} M. Oxygen was bubbled in the cuvette for 10 min. The solution was then irradiated with visible light ($\lambda > 390$ nm) and the reaction was followed by acquiring UV-vis absorption spectra at different times. The same procedure was followed for the photoreactions involving other photosensitizers, *i.e.* [Re(phen)$(CO)_3$(py)]OTf (1×10^{-5} M), and methylene blue (MB, 8×10^{-7} M, the much lower concentration being necessary to balance the much higher molar absorptivity of MB).

2.6. Cell uptake and cytotoxicity in dark and light conditions

SPIO@SiO_2–Re@PEG-NPs were sonicated 30 minutes at 40 kHz (Sonica – Soltec) just before the use in order to obtain a homogenous dispersion and then different volumes of the stock suspension were added directly in the culture medium to obtain the working concentrations. The alveolar epithelial cells A549 from human lung carcinoma, purchased from ECACC (European Collection of Cell Cultures), were routinely maintained in OptiMEM 10% FBS, at 37 °C, 5% CO_2 and seeded in 6 multi-well plates for the cell uptake assays. Images of treated-cells were recorded after exposure for 4 h or 24 h to: (a) 50 μL of a 760 μg mL^{-1} suspension of NPs affording a NP concentration of 19 μg mL^{-1}, corresponding to a [Re] = 0.95 μM in the well; (b) 50 μL of a water solution (3.2×10^{-4} M) of the precursor molecule [Re(phen)$(CO)_3$(py-upts)]OTf, affording a final [Re] = 8.0 μM in the well. Two photon excitation at 840 nm was exploited (with an excitation power on the sample of about 15 mW).

The A549 cells were also seeded in 12 multi-well plates for cell viability evaluation. Cells were exposed to increasing concentrations of NPs (1.9; 9.5; 19; 38; 76 μg mL^{-1}) and then incubated for 4 h at 37 °C, 5% CO_2 to allow NP internalization. At the end of this pre-incubation period the A549 cells were irradiated with the 150 W/NDL lamp light (200 mW cm^{-2}) for 10 min in order to photoactivate the internalized nanostructured compound and then they were incubated again for 3 h or 16 h. Not irradiated cells exposed at the same concentrations of NPs were used as reference (dark conditions). At the end of the exposure, cells were rinsed with PBS and the working MTT solution prepared in culture medium at a concentration of 0.3 mg mL^{-1} was added. After 2 h the MTT solution was removed and the purple MTT reduction product (formazan salts) was solubilized with DMSO. The optical density of each sample, proportional to cell viability, was measured at 570 nm using 690 nm as reference wavelength with a multiplate reader. The experiments were replicated three times and results were expressed as mean ± SE. Statistical differences were verified using One way ANOVA followed by Fischer LSD test ($p < 0.05$).

3. Results and discussion

3.1. Synthesis of the complex [Re(phen)$(CO)_3$(py-upts)]OTf

As discussed in the Introduction, a $[Re(phen)(CO)_3(py)]^+$ complex has been chosen as luminescent probe and singlet oxygen photosensitizer. In order to avoid its slow release from the inorganic matrix, the pyridine ligand was functionalized with a triethoxysilane moiety, to covalently bind the complex to the silica shell. The ligand 1-(pyridin-4-yl)-3-(3-(triethoxysilyl) propyl)urea,[46] hereafter py-upts, was obtained as depicted in Scheme 1, using a slightly modified literature procedure.[47]

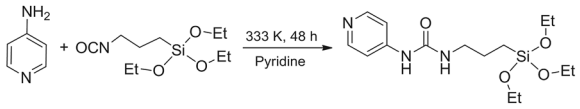

Scheme 1 Reaction scheme for the synthesis of the py-upts ligand.

Then the [Re(phen)(CO)$_3$(py-upts)]OTf complex was prepared, by replacing with py-upts the labile triflate ligand in the precursor [Re(phen)(CO)$_3$(OTf)] complex (Scheme 2).[48] The reaction was carried out in anhydrous ethanol, to avoid the early hydrolysis of the three ethoxy groups of the silane moiety, and its progress was monitored by ^{1}H NMR (Fig. S3†). The entry of pyridine in the ligand sphere was accompanied by the progressive shift of the photoluminescence, from a faded orange to a brilliant yellow color.

3.2. Synthesis of the magneto-optical SPIO@SiO$_2$–Re@PEG nanocomposites

The synthesis of iron oxide NPs stabilized by an oleic acid shell was performed by a literature procedure,[50] involving thermal decomposition of iron oleate in a high boiling solvent (here 1-octadecene). NPs with a diameter size distribution centered at 10.4 ± 1.3 nm (from DLS analysis, Fig. S4†) were obtained. The transmission electron microscopy (TEM) images (Fig. 1) were in good agreement with the DLS data, showing a size distribution of the magnetic core centred at 9.4 ± 1.3 nm.

The silica shell was grown in a reverse microemulsion environment,[51,52] and the reaction was stopped after 6 h, when DLS indicated the prevalence of NPs with a hydrodynamic diameter of about 45 nm (Fig. S5†).

The luminescent [Re(phen)(CO)$_3$(py-upts)]OTf complexes were then anchored to the silica shell, by treating the SPIO@SiO$_2$ NPs, dispersed in ethanol, with an ethanol solution of the complex, as depicted in the second step of Scheme 3. The mixture was refluxed for 5 h, and the precipitate was recovered by centrifugation (see Experimental part). The solid was strongly luminescent and was also attracted by an external permanent magnet (Fig. S6†), thus immediately indicating the formation of a dual magneto-luminescent nano-system (as subsequently demonstrated by the detailed characterization described in the following sections).

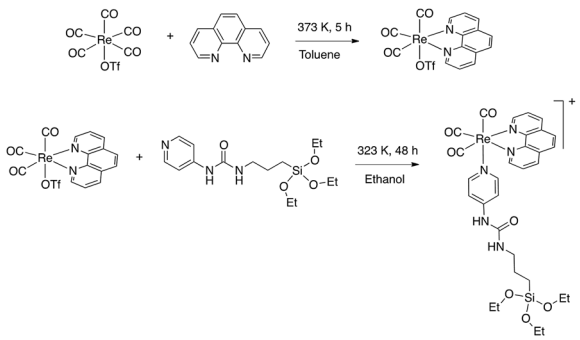

Scheme 2 Synthetic route to the complex [Re(phen)(CO)$_3$(py-upts)]OTf.

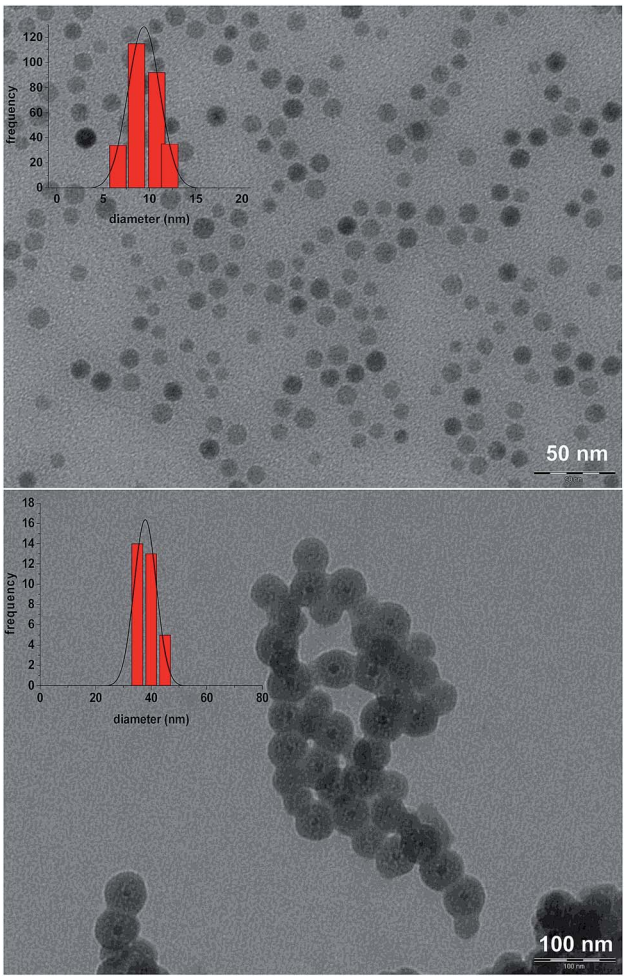

Fig. 1 TEM micrograph of the SPIO@OA NPs (up) and of the core/shell SPIO@SiO$_2$–Re@PEG NPs (down), with the corresponding size distribution histograms.

Attempts to insert the luminescent probe directly in the water-in-oil microemulsion, to condense its silane terminals to the SPIO@SiO$_2$ inside the nanoreactor, failed, since significant aggregation was observed, likely due to destabilization of the microemulsion after the treatment with the ethanol solution of the Re complex.

Upon water addition the SPIO@SiO$_2$-Re NPs were easily suspended, but the stability of the colloidal dispersion was poor and in few hours the NPs completely settled. For this reason, and also to make them stealth to the reticulo-endothelial system for any *in vivo* future use, the NPs were stabilized by capping their surface with short polyethylene glycol molecules (last step in Scheme 3), previously functionalized with a triethoxysilane group through a carbamate link (Scheme 4 and Fig. S7†).[53] After the coating with the PEG$_{500}$-silane, the ζ potential of the NPs changed from −20 mV to 0 mV and the hydrodynamic diameter increased from 45 nm to about 80 nm (Fig. S8†). Moreover, the thermogravimetric analysis of the nanocomposite (Fig. S9†) revealed an overall loss weight of about 60%, ascribable to PEG and to the ligands on the rhenium complex.

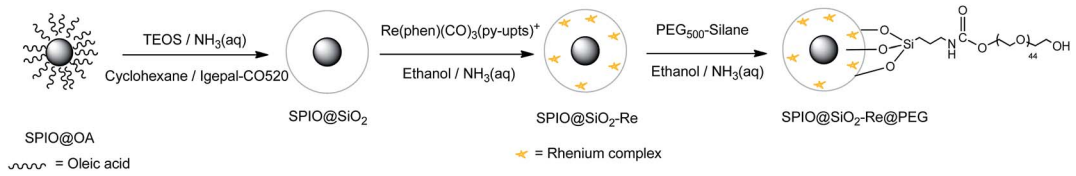

Scheme 3 Schematic steps diagram of the synthesis of PEG-capped magneto-luminescent SPIO@SiO_2–Re@PEG NPs.

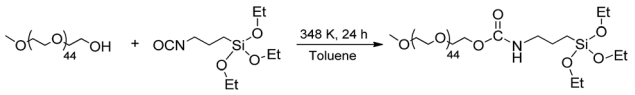

Scheme 4 The preparation of the PEG silanized by formation of a carbamate link.

The presence of the polymer shell strongly improved the stability of the colloid and reduced the formation of irreversibly aggregated NPs.

The morphology of the magneto-luminescent SPIO@SiO_2–Re@PEG nanocomposite was analyzed by TEM (Fig. 1), which revealed a spherical form and a single magnetic core per core/shell nanocomposite. The size distribution of the nanocomposite showed a single population centered at 40 ± 3.5 nm.

The amount of Re on the NPs was estimated by ICP-AES analysis, corresponding to a loading of *ca.* 6000 Re atoms per NPs. This loading well compares with the one obtained for related Ru luminescent complexes covalently embedded into silica NPs with diameters of *ca.* 60 nm (4600 Ru atoms per NP).[54]

3.3. Photoluminescence properties of the precursor Re complex and of the SPIO@SiO_2–Re@PEG NPs

The photophysical characterization of the free complex [Re(phen)$(CO)_3$(py-upts)]OTf and of the corresponding SPIO@SiO_2–Re@PEG nanocomposite was performed in dilute, air equilibrated, water solution (about 1.0×10^{-5} M), as well as in the solid state. In order to evaluate the influence of the urea link in the *para* position of the pyridine ligand, the photophysical properties of the precursor complex were compared with those of the already known [Re(phen)$(CO)_3$(py)]OTf complex[16] containing the unsubstituted pyridine ligand. The most relevant photophysical data are listed in Table 1 and the corresponding absorption and emission spectra are displayed in Fig. 2.

The UV-vis absorption spectra of the free complexes and the NPs showed a strong band at about 275 nm, ascribed to ligand-centered (LC) π–π^* transitions, and a weaker broad band, centered at about 370 nm. The latter band is ascribable to a spin allowed dπ(Re) $\rightarrow$ π^*(phen) metal-to-ligand charge transfer transition (^{1}MLCT), by comparison with analogous cationic Re(I) tricarbonyl complexes.[15,16]

Upon optical excitation the free complexes displayed a broad and featureless emission band in the green-yellow region of the visible spectrum, arising from an excited state that can be described as a triplet MLCT state.[12] This was confirmed by the quenching of the emission on going from de-aerated to air equilibrated solution (yields dropping from 0.117 to 0.070 for [Re(phen)$(CO)_3$(py)]OTf, and from 0.053 to 0.038 for [Re(phen)$(CO)_3$(py-upts)]OTf) and by the solvent-dependence of the emission maximum, which results red-shifted by about 20 nm on going from CH_2Cl_2 ($\lambda = 544$ nm)[16] to water ($\lambda = 567$ nm, Table 1) for the complex [Re(phen)$(CO)_3$(py)]OTf.

The MLCT nature of the excited state was further supported by the influence of the pyridine substituents on the absorption and emission spectra. Actually, the introduction of the electron-donating (by resonance effect) urea link in the *para* position of the pyridine ligand, afforded a red-shift of about 13 nm of the emission maximum of [Re(phen)$(CO)_3$(py-upts)]OTf with respect to [Re(phen)$(CO)_3$(py)]OTf. This is in line with the presence of the electron-richer py-upts ancillary ligand,[55] which raises the HOMO level, then lowering the energy of the MLCT transition. The red shift of the emission energy, observed for the complex [Re(phen)$(CO)_3$(py-upts)]OTf, was accompanied by a slight decrease of the photoluminescence quantum yield (Φ) and of the lifetime of the excited state (Table 1), in agreement with the energy gap law.[56]

Table 1 Photoluminescence data for the molecular Re complexes and for the SPIO@SiO_2–Re@PEG NPs, in aerated water solution and in solid state (room temperature, $\lambda_{ex} = 375$ nm)

	Water solution, air			Solid		
Compound	λ_{em}/nm	τ/ns	Φ	λ_{em}/nm	τ/ns	Φ
[Re(phen)$(CO)_3$(py)]OTf	567	454	0.070	530	740 (46%) 2570 (54%)	0.158
[Re(phen)$(CO)_3$(py-upts)]OTf	580	257	0.038	553	993 (30%) 2032 (70%)	0.119
SPIO@SiO_2–Re@PEG NPs	553	409 (22%) 1738 (78%)	0.060			

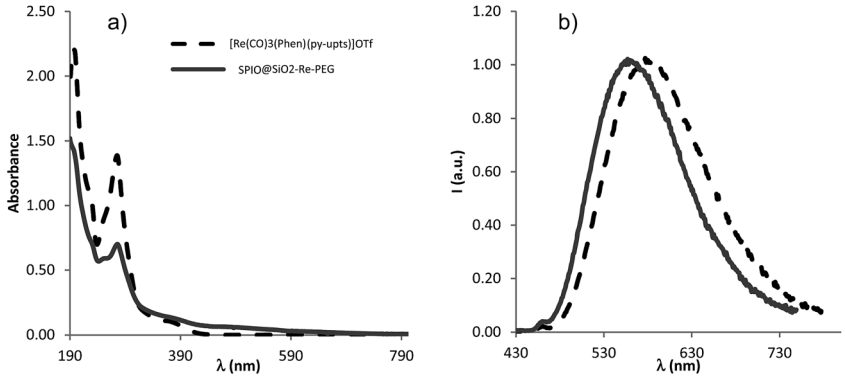

Fig. 2 (a) UV-vis absorption and (b) normalized photoluminescence spectra ($\lambda_{ex} = 375$ nm) of [Re(phen)(CO)$_3$(py-upts)]OTf (black dashed traces) and SPIO@SiO$_2$–Re@PEG NPs (gray traces) in air equilibrated water solution at room temperature.

The photophysical properties of the complexes were investigated also in the solid state, showing a blue shift of the emission maxima with respect to the solution, in agreement with the rigidochromic effect usually observed for mononuclear rhenium complexes.[57] An increase of the Φ values was also observed, indicating that here the quenching processes often observed in the solid state do not occur, and the dominant effect is the decrease, in the rigid environment, of the roto-vibrational motions, responsible for the non-radiative deactivation pathways of the excited states.[17a,c]

Some interesting differences in the photophysical behavior were observed on going from the molecular complexes to the NPs. The emission maximum of the NPs in water solution was considerably blue-shifted with respect to the corresponding [Re(phen)(CO)$_3$(py-upts)]$^+$ complex in the same conditions, to a value very similar to the one measured for this complex in the solid state. Moreover, for the NPs the excited state lifetimes were longer and the emission quantum yields higher than the values measured for the corresponding py-upts complex in solution. This can be attributed both to the confinement of the complex in the rigid silica environment and to its poor exposition to the solution, hampering the deactivating action of water. However, the complex in the (porous) silica shell remained sensitive to oxygen presence, as indicated by its ability to generate singlet oxygen (see paragraph 3.6).

The two excited state lifetimes observed for the NPs, as well as for the complexes in the solid state, result from the presence of complexes experiencing different environments, with different available non-radiative deactivation pathways.

3.4. Relaxometry properties of SPIO@SiO$_2$–Re@PEG NPs

The ^{1}H NMR longitudinal and transverse relaxation times of the SPIO@SiO$_2$–Re@PEG NPs were measured at room temperature in the frequency range to cover most of the typical fields for MRI tomographs, used both in clinics ($H = 0.2$, 0.5, and 1.5 T) and in research laboratories,[58] as specified in the experimental part. The efficiency of the contrast agents was evaluated in the usual way: the nuclear relaxivities, both r_1 and r_2, were calculated as the inverse of the relaxation times normalized for contrast agent concentration, *i.e.* the concentration of the magnetic part, once previously corrected for the host diamagnetic contribution, according to eqn (2).

$$r_i = [(1/T_i)_{meas} - (1/T_i)_{dia}]/c,\ i = 1, 2 \quad (2)$$

where $(1/T_i)_{meas}$ is the measured value on the sample with iron concentration $c = 0.119$ mmol L^{-1}, and $(1/T_i)_{dia}$ refers to the nuclear relaxation rate of the milliQ water used as host solution.

Fig. 3 shows the r_1 and r_2 nuclear relaxivities of SPIO@SiO$_2$–Re@PEG NPs together with the values for the commercial contrast agent Endorem®. The displayed r_2 values for $\upsilon > 5$ MHz ($r_2 > 30$ s^{-1} mM^{-1}) guarantee an appreciable contrast in the MR

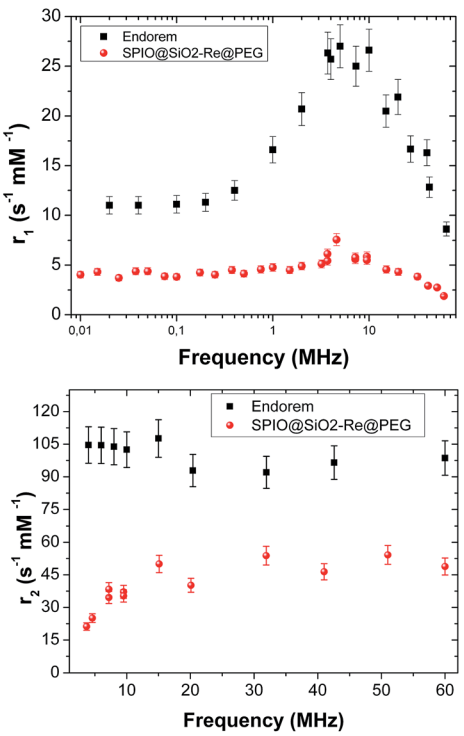

Fig. 3 Longitudinal (top) and transverse (bottom) relaxivities of SPIO@SiO$_2$–Re@PEG NPs (red circles) dispersed in water. Data are compared with the commercial compound Endorem® values (black squares).

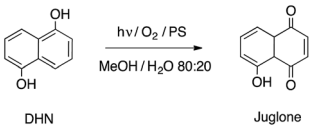

Scheme 5 Photochemical oxidation of DHN to juglone in the presence of a photosensitizer (PS).

images once the nanoparticles are used, as some of us already demonstrated on other T_1 and/or T_2 relaxing nanoparticles of completely different types.[59]

3.5. Singlet oxygen generation by SPIO@SiO$_2$–Re@PEG NPs

The photochemical stability of the photosensitizer was preliminarily tested, by irradiating for 1 h a sample of the free complex [Re(phen)(CO)$_3$(py-upts)]OTf, dissolved in water saturated with O_2 (Fig. S2†). The superposition of the absorption spectra recorded at different times indicated the high photostability of the photosensitizer in these conditions.

The efficiency of the SPIO@SiO$_2$–Re@PEG NPs toward singlet oxygen generation was assessed by using 1,5-dihydroxynaphthalene (DHN) as indirect marker of the $^1O_2$ presence. Actually, DHN reacts quantitatively with $^1O_2$ to give the oxidized species juglone (5-hydroxy-1,4-naphtalenedione, Scheme 5), according to eqn (3).[35,60,61]

$$\mathrm{DHN} + {}^1\mathrm{O}_2 \rightarrow \mathrm{juglone} + \tfrac{1}{2}{}^3\mathrm{O}_2 \qquad (3)$$

Thus, the $^1O_2$ production was indirectly monitored by following the decrease of the UV-vis absorption band of DHN at 297 nm (accompanied by the increase of the juglone band at 427 nm). Fig. 4A shows the spectra recorded for the first 60 min of irradiation of a sample of NPs suspended in a MeOH/H$_2$O (80 : 20) mixture, in the presence of DHN.

The reaction in the initial stages follows a pseudo-first order kinetics, $v = k_{obs}[DHN]$, provided that the oxygen concentration within this interval of time can be considered constant.[61] By plotting as a function of the irradiation time the values of $\ln(A/A_0)$ for the DHN absorption at 297 nm (Fig. 4B), the kinetic constant k_{obs} for reaction 3 can be estimated.

The reaction was also carried out employing as photosensitizers the precursor complex [Re(phen)(CO)$_3$(py-upts)]OTf, or the analogue [Re(phen)(CO)$_3$(py)]OTf complex (for comparison), and methylene blue (MB) as standard.

The quantum yields for singlet oxygen generation (Φ_Δ) were determined using eqn (4):

$$\Phi_\Delta = \Phi_\Delta^{std} \times (v_i I^{std}/v_i^{std} I) \qquad (4)$$

where v_i is the initial rate of reaction (3), I indicates the photons absorbed by the sensitizer, and the apex std labels the corresponding values for the standard (methylene blue in our case, $\Phi_\Delta = 0.50$ in MeOH).[62] The values of v_i were provided by the product $k_{obs}[DHN]_i$ ($[DHN]_i$ being 1×10^{-4} M), while the values of I were estimated by numerical integration of $I_{source}(\lambda)$ $(1-10^{A(\lambda)})$, where $I_{source}(\lambda)$ is the intensity of the incident light at different wavelengths and $A(\lambda)$ is the corresponding absorbance of the considered sensitizer.

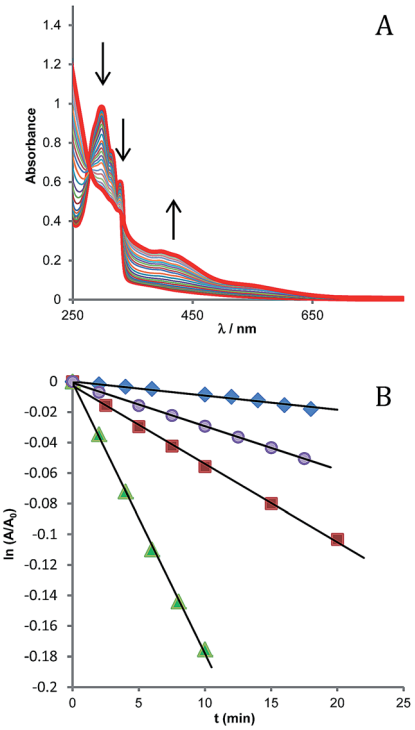

Fig. 4 (A) UV-vis absorption spectra recorded at different irradiation times (from 0 to 360 min, λ > 390 nm) on a solution containing SPIO@SiO$_2$–Re@PEG NPs (150 μg mL^{-1}) and DHN (10^{-4} M) in 2.5 mL of MeOH/H$_2$O (80/20) bubbled with O_2 for 10 min. (B) Photo-oxidation of DHN in the presence of different sensitizers: methylene blue (△), [Re(phen)(CO)$_3$(py)]OTf (○), [Re(phen)(CO)$_3$(py-upts)]OTf (□), and SPIO@SiO$_2$–Re@PEG NPs (◇). A_t and A_0 represent the absorbance measured at 297 nm (the maximum of the DHN absorption band) at time t and time 0, respectively.

It must be pointed out that the Φ_Δ values estimated for dyes entrapped into nano-supports are affected by significant uncertainties, because of the extinction arising from light scattering (which varies with wavelength and can be only partly corrected)[63] and also because of many other possible matrix effects (including here the absorption of the iron oxide core), which are difficult to accurately evaluate.[64] All these contributions to the absorption spectra do not contribute to the excitation of the sensitizer, and therefore their inclusion in the computation of the I value can lead to severe underestimation of the quantum yields. For these reasons we preferred to obtain an approximate value of the photons absorbed by the rhenium dye in the NPs by using the absorption spectrum of the free complex, corrected for the different concentrations in the two solutions (that were known from the ICP analysis of the rhenium content).

The Φ_Δ values estimated in this way for the SPIO@SiO$_2$–Re@PEG NPs resulted very similar to the ones evaluated for the free Re complexes (0.26–0.29, see Table 2), which well compare with those reported for analogous tricarbonyl Re complexes (0.20–0.26) in water solution.[20,65] Due to the approximations involved in the evaluation of the light absorbed by the Re

Table 2 Pseudo first-order kinetics parameters and $^1O_2$ generation quantum yields for the photooxidation of DHN using the standard MB, the molecular complexes and the SPIO@SiO_2–Re@PEG NPs, in oxygenated water solution. Initial DHN concentration = 1×10^{-4} M. The values for the NPs are in parentheses because evaluated by the approximation described in the text

	$k_{obs} \times 10^3$ (min^{-1})	I (mW cm^{-1})	Φ_Δ
Methylene blue	17.8	4.63	0.50
[Re(phen)$(CO)_3$(py-upts)]OTf	5.30	2.64	0.26
[Re(phen)$(CO)_3$(py)]OTf	2.91	1.31	0.29
SPIO@SiO_2–Re@PEG NPs	0.925	(0.57)	(0.21)

complexes on the NPs, we cannot rule out that the actual quantum yields were somewhat lower than reported in Table 2. In fact some decrease of the Φ_Δ value might result from the fact that $^3O_2$ has to diffuse across the NP coating in order to quench the triplet excited state of the anchored dyes and from the possibility of entrapment of generated $^1O_2$ in the NP matrix. However, the significant point is that the NPs do maintain a significant sensitizing activity. A lowest limit to this activity ($\Phi_\Delta = 0.05$) was computed using the unprocessed absorption spectra of the SPIO@SiO_2–Re@PEG NPs, *i.e.* the spectrum including all the ineffective contributions.

This is remarkably different from what observed for a very effective sensitizer as MB, for which a strong decrease in the $^1O_2$ release (about two order of magnitude) when entrapped in a silica layer was measured in a previous work.[67] This might be due to some triplet–triplet annihilation process, arising from the close spatial confinement of a large number of emitters with very long excited state lifetimes, as it is typical of the triplet states of organic dyes. On the contrary, for the rhenium complex, which has a relatively short lifetime of the triplet state, the efficiency in singlet oxygen generation was maintained.

3.6. Cell uptake and PDT cytotoxicity of the SPIO@SiO_2–Re@PEG nanoparticles

The cell uptake of the nanocomposites was preliminarily investigated, to find the time scale useful for the PDT assays. The uptake by A549 cells was monitored by confocal microscopy, exploiting the photoluminescence of the Re complexes, and in particular the possibility to promote their emission by two-photon excitation (TPE). TPE microscopy (as described first by Denk *et al.*)[68] uses near-infrared laser light to excite chromophores with a (non-linear) quadratic dependence of the excitation probability from the laser power, inducing optical sectioning without the need of a pinhole (spatial filter). It presents many advantages for *in vivo* applications: the near-infrared light displays a deeper penetration in highly scattering tissues, and it induces a much lower photodamage of the sample with respect to UV radiation. The intrinsic optical sectioning, moreover, limits the possible phototoxic effect to the focal plane only, and increases the detection efficiency of the whole system, since it does not require descanning optics nor pinholes in the revelation path, allowing the use of large active area detectors.

Cells were incubated either with the molecular probe [Re(phen)$(CO)_3$(py-upts)]OTf or with the SPIO@SiO_2–Re@PEG NPs, at different concentrations (see Experimental), and observed after both 4 h and 24 h through TPE confocal microscopy. Nuclei were stained with the viable nuclear dye Hoechst (blue), just before the microscopy evaluation.

The internalization of the free Re complex was hampered by its low solubility in aqueous media, which led to the formation of microsized aggregates, well visible in the images acquired after 4 h of incubation (Fig. S10A†). However, a moderate cell uptake was observed at longer times (24 h, Fig. S10B†), and the complexes accumulated in the cytoplasm, forming small endosomal-like clusters.

On the contrary, the nanoparticles were more easily internalized and accumulated in the perinuclear region of the cells already after 4 h of incubation (see Fig. 5B and the movie of a z-scan images sequence, downloadable from ESI†), although their persistence in the cytoplasm at longer times was not confirmed. The feeble luminescence observed after 24 h (Fig. 5C) was mainly localized outside the cell membranes, suggesting that most of the probes had been excreted by the cells. On the bases of these results an incubation time of 4 h was set for the cytotoxicity assays.

The cytotoxic effect of the SPIO@SiO_2–Re@PEG NPs was assessed both in dark and light conditions, to investigate the ability of the NPs to induce an increase in cell death when photo-activated. Cells were incubated with different concentrations of NPs for 4 h, then were either irradiated for 10 min with light from a 150 W NDL lamp or kept in the dark for the same time, and finally incubated again for 3 h or 16 h. At the

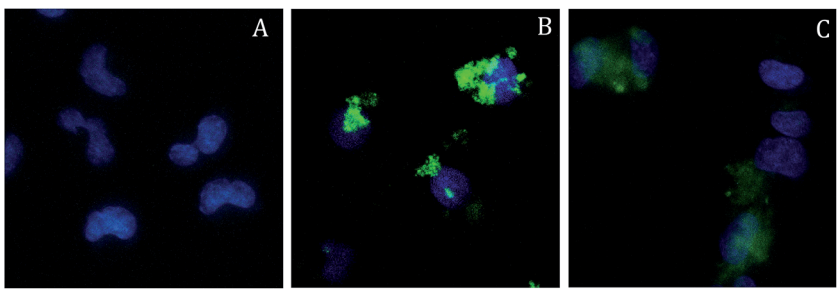

Fig. 5 TPE microscopy images, result of the projection and superposition on the *xy* plane of 10 single planes acquired along the *z* axis at 0.5 μm steps, of A549 cells incubated with SPIO@SiO_2–Re@PEG NPs (19 μg mL^{-1}, corresponding to [Re] = 0.95 μM) for 4 h (panel B) and 24 h (panel C). Panel A shows untreated A549 cells used as control for the same experiment. The blue color is due to the staining of nuclei with Hoechst.

end, the cell viability was evaluated by the MTT test (see Experimental part).

The results are summarized in Fig. 6. After 3 h and 16 h post irradiation (p.i.), a dose dependent effect induced by the NPs was observed, with a statistically significant increase in cell mortality after irradiation of the cells, compared to the dark exposure, testifying for an effective photodynamic response.

The slight cytotoxic effect observed for cells exposed to the highest NP concentrations in the dark should be attributed to the whole nanostructure, rather than to the sensitizer (*i.e.* the Re complex). Indeed the [Re(phen)$(CO)_3$(py-upts)]OTf complex alone did not induce any cytotoxicity, as shown by viability tests performed by exposing A549 cells for different times (4 h or 24 h) to increasing concentrations of the complex (see Fig. S11†).

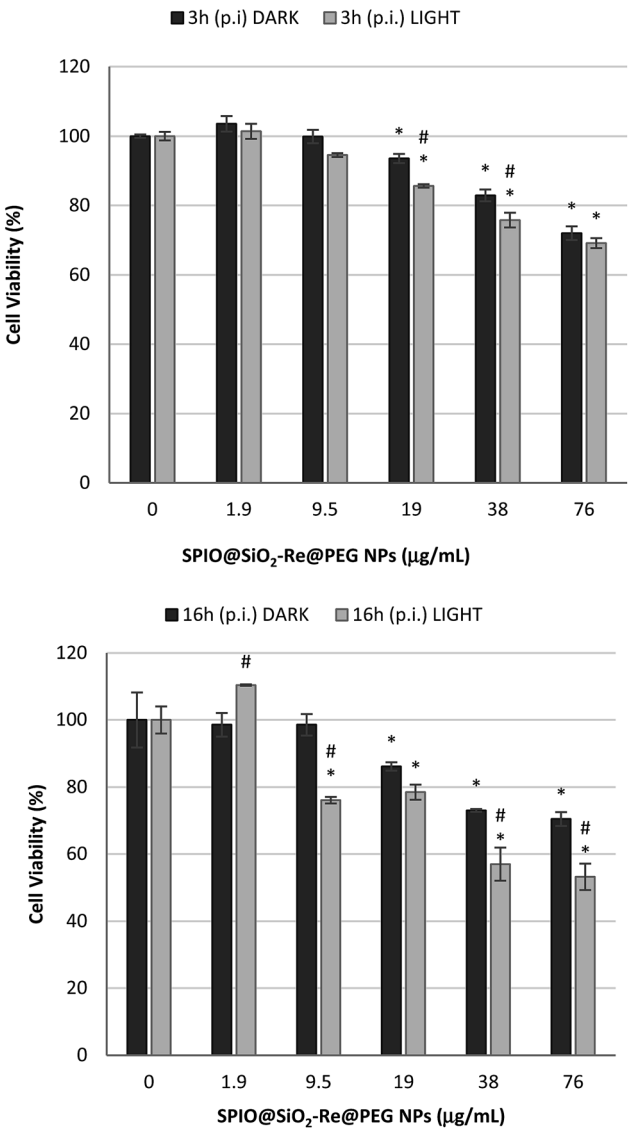

Fig. 6 Cell viability (MTT assay) of A549 cells exposed to SPIO@SiO_2–Re@PEG NPs for 3 h and 16 h post irradiation (p.i.). Black bars = dark conditions; grey bars = light conditions: cells were exposed to NPs for 4 h, irradiated for 10 min and incubated for 3 h or 16 h again. *Significantly different from control; #significantly different light *vs.* dark conditions (ANOVA + Fischer LSD test, $p < 0.05$).

4. Conclusions

A multifunctional nanocomposite, designed for being a bimodal imaging probe that can be exploited also for PDT, has been prepared and characterized. As shown by the results, each component of the nanocomposite preserved the ability to perform its function. The superparamagnetic iron oxide cores, coated by the thick layer of silica and by PEG, to improve stability and stealthiness in physiological conditions, remained able to act as T2 agents for MRI, providing a good contrast ability, as demonstrated by the relaxivity profiles.

At the same time, the luminescence properties, as lifetimes and photoluminescence quantum yields, were even improved by the entrapment of the emitting rhenium complex in the silica shell, due to increased rigidity of the environment and to reduced interaction with the water. Finally, the Re complexes anchored to the NPs were still able to act as effective $^1O_2$ photosensitizer.

Preliminary investigation has revealed easy cellular uptake and increased cytotoxicity upon irradiation with respect to the dark, even if with a low efficiency. This might be related to the NP localization at subcellular level, which is known to have strong influence on cell response to photoactivation.[21,24,69] Further studies on the internalization mechanism and on the subcellular localization will be necessary to assess the true potential of these nanocomposites. In a parallel way the performances of the diagnostic and therapeutic functionalities integrated in the SPIO@SiO_2–Re@PEG NPs can be optimized: the T2 contrast ability would benefit from a larger size of the superparamagnetic core and a smaller thickness of the silica shell, while the luminescence properties as well as the capability of $^1O_2$ generation would be improved by an increased Re loading.

Acknowledgements

The use of instrumentation purchased through the Regione Lombardia – Fondazione Cariplo joint SmartMatLab Project (2013-1766) is gratefully acknowledged. The authors also thank INSTM-Regione Lombardia (project MAGNano) for funding.

Notes and references

1 See for instance: (*a*) G. Chen, I. Roy, C. Yang and P. N. Prasad, *Chem. Rev.*, 2016, **116**, 2826–2885; (*b*) X. Chen, S. S. Gambhir and J. Cheon, Special issue, Theranostic Nanomedicine, *Acc. Chem. Res.*, 2011, **44**, 841–1134.
2 E. Duguet, S. Vasseur, S. Mornet and J.-M. Devoisselle, *Nanomedicine*, 2006, **1**, 157–168.
3 A. K. Gupta and A. S. Curtis, *J. Mater. Sci.: Mater. Med.*, 2004, **15**, 493–496.
4 K. Ding, L. H. Jing, C. Y. Liu, Y. Hou and M. Y. Gao, *Biomaterials*, 2014, **35**, 1608–1617.
5 G. N. Wang, L. Jin, Y. K. Dong, L. Niu, Y. X. Liu, F. Ren and X. G. Su, *New J. Chem.*, 2014, **38**, 700–708.
6 G. N. Wang and X. G. Su, *Analyst*, 2011, **136**, 1783–1798.

7 J. H. Lee, Y. W. Jun, S. I. Yeon, J. S. Shin and J. Cheon, *Angew. Chem., Int. Ed.*, 2006, **45**, 8160–8162.
8 Z. Ali, A. Z. Abbasi, F. Zhang, P. Arosio, A. Lascialfari, M. F. Casula, A. Wenk, W. Kreyling, R. Plapper, M. Seidel, R. Niessner, J. Knoll, A. Seubert and W. J. Parak, *Anal. Chem.*, 2011, **83**, 2877–2882.
9 Q. Ma, Y. Nakane, Y. Mori, M. Hasegawa, Y. Yoshioka, T. M. Watanabe, K. Gonda, N. Ohuchi and T. Jin, *Biomaterials*, 2012, **33**, 8486–8494.
10 W. Jiang, K. L. Lai, K. X. Liu, R. Xia, F. B. Gao, Y. Wu and Z. W. Gu, *Nanoscale*, 2014, **6**, 1305–1310.
11 (*a*) M. P. Coogan and V. Fernandez-Moreira, *Chem. Commun.*, 2014, **50**, 384–399; (*b*) E. Baggaleya, J. A. Weinsteina and J. A. G. Williams, *Coord. Chem. Rev.*, 2012, **256**, 1762–1785; (*c*) K. K.-W. Lo, M.-W. Louie and K. Y. Zhang, *Coord. Chem. Rev.*, 2010, **254**, 2603–2622; (*d*) H. Xiang, J. Cheng, X. Ma, X. Zhou and J. J. Chruma, *Chem. Soc. Rev.*, 2013, **42**, 6128–6185; (*e*) F. L. Thorp-Greenwood, R. G. Balasingham and M. P. Coogan, *J. Organomet. Chem.*, 2012, **714**, 12–21; (*f*) E. Licandro, M. Panigati, M. Salmain and A. Vessières, in *Bioorganometallic Chemistry: Applications in Drug Discovery, Biocatalysis, and Imaging*, ed. G. Jaouen and M. Salmain, Wiley-VCH, Weinheim, 2015, pp. 341–391.
12 For some pertinent reviews, see: (*a*) A. Kumar, S.-S. Sun and A. J. Lees, *Top. Organomet. Chem.*, 2010, **29**, 1–35; (*b*) D. R. Striplin and G. A. Crosby, *Coord. Chem. Rev.*, 2001, **211**, 163–175; (*c*) D. J. Stukfens Jr and A. Vlček, *Coord. Chem. Rev.*, 1998, **177**, 127–179; (*d*) A. J. Lees, *Chem. Rev.*, 1987, **87**, 711–743.
13 See, for instance: (*a*) H. C. Bertrand, S. Clède, R. Guillot, F. Lambert and C. Policar, *Inorg. Chem.*, 2014, **53**, 6204–6223; (*b*) V. Fernández-Moreira, I. Marzo and M. C. Gimeno, *Chem. Sci.*, 2014, **5**, 4434–4446; (*c*) F. L. Thorp-Greenwood, M. P. Coogan, L. Mishra, N. Kumari, G. Rai and S. Saripella, *New J. Chem.*, 2012, **36**, 64–72; (*d*) C. Mari, M. Panigati, L. D'Alfonso, I. Zanoni, D. Donghi, L. Sironi, M. Collini, S. Maiorana, C. Baldoli, G. D'Alfonso and E. Licandro, *Organometallics*, 2012, **31**, 5918–5928; (*e*) G. Gasser, A. Pinto, S. Neumann, A. M. Sosniak, M. Seitz, K. Merz, R. Heumann and N. Metzler-Nolte, *Dalton Trans.*, 2012, **41**, 2304–2313; (*f*) M.-W. Louie, T. T.-H. Fong and K. K.-W. Lo, *Inorg. Chem.*, 2011, **50**, 9465–9471; (*g*) K. K. W. Lo, K. Y. Zhang and S. P. Y. Li, *Eur. J. Inorg. Chem.*, 2011, **24**, 3551–3568; (*h*) E. Ferri, D. Donghi, M. Panigati, G. Prencipe, L. D'Alfonso, I. Zanoni, C. Baldoli, S. Maiorana, G. D'Alfonso and E. Licandro, *Chem. Commun.*, 2010, **46**, 6255–6257; (*i*) M.-W. Louie, T. T.-H. Fong and K. K.-W. Lo, *Inorg. Chem.*, 2011, **50**, 9465–9471; (*j*) S. James, K. P. Maresca, J. W. Babich, J. F. Valliant, L. Doering and J. Zubieta, *Bioconjugate Chem.*, 2006, **17**, 590–596; (*k*) K. K.-W. Lo, K. H.-K. Tsang and N. Zhu, *Organometallics*, 2006, **25**, 3220–3227; (*l*) S. J. Reece, M. R. Seyedsayamdost, J. Stubbe and D. G. Nocera, *J. Am. Chem. Soc.*, 2006, **128**, 13654–13655; (*m*) K. K.-W. Lo, W.-K. Hui, C.-K. Chung, K. H.-K. Tsang, T. K.-M. Lee, C.-K. Li, J. S.-Y. Lau and D. C.-M. Ng, *Coord. Chem. Rev.*, 2006, **250**, 1724–1736.
14 (*a*) M. Mauro, C.-H. Yang, C.-Y. Shin, M. Panigati, C.-H. Chang, G. D'Alfonso and L. De Cola, *Adv. Mater.*, 2012, **24**, 2054–2058; (*b*) X. Li, D. Zhang, H. Chi, G. Xiao, Y. Dong, S. Wu, Z. Su, Z. Zhang, P. Lei, Z. Hu and W. Li, *Appl. Phys. Lett.*, 2010, **97**, 263303–263306; (*c*) M. Mauro, E. Quartapelle Procopio, Y. Sun, C.-H. Chien, D. Donghi, M. Panigati, P. Mercandelli, P. Mussini, G. D'Alfonso and L. De Cola, *Adv. Funct. Mater.*, 2009, **19**, 2607–2614; (*d*) C. Cebrián, M. Natali, D. Villa, M. Panigati, M. Mauro, G. D'Alfonso and L. De Cola, *Nanoscale*, 2015, **7**, 12000–12009.
15 (*a*) J. M. Villegas, S. R. Stoyanov, W. Huang and D. P. Rillema, *Inorg. Chem.*, 2005, **44**, 2297–2309; (*b*) W.-M. Xue, N. Goswami, D. M. Eichhorn, P. L. Orizondo and D. P. Rillema, *Inorg. Chem.*, 2000, **39**, 4460–4467.
16 (*a*) L. Sacksteder, A. P. Zipp, E. A. Brown, J. Streich, J. N. Demas and B. A. DeGraff, *Inorg. Chem.*, 1990, **29**, 4335–4340; (*b*) L. Wallace and D. P. Rillema, *Inorg. Chem.*, 1993, **32**, 3836–3843.
17 (*a*) M. Panigati, D. Donghi, M. Mauro, P. Mercandelli, P. Mussini, L. De Cola and G. D'Alfonso, *Coord. Chem. Rev.*, 2012, **256**, 1621–1643; (*b*) Y.-H. Tseng, D. Bhattacharya, S.-H. Lin, P. Thanasekaran, J.-Y. Wu, L.-W. Lee, M. Sathiyendiran, M.-L. Ho, M.-W. Chung, K.-C. Hsu, P.-T. Chou and K.-L. Lu, *Inorg. Chem.*, 2010, **49**, 6805–6807; (*c*) E. Quartapelle Procopio, M. Mauro, M. Panigati, D. Donghi, P. Mercandelli, A. Sironi, G. D'Alfonso and L. De Cola, *J. Am. Chem. Soc.*, 2010, **132**, 14397–14399; (*d*) D. Donghi, G. D'Alfonso, M. Mauro, M. Panigati, P. Mercandelli, A. Sironi, P. Mussini and L. D'Alfonso, *Inorg. Chem.*, 2008, **47**, 4243–4255.
18 S. Carron, M. Bloemen, L. Vander Elst, S. Laurent, T. Verbiest and T. N. Parac-Vogt, *J. Mater. Chem. B*, 2015, **3**, 4370–4376.
19 K. Wähler, A. Ludewig, P. Szabo, K. Harms and E. Meggers, *Eur. J. Inorg. Chem.*, 2014, 807–811.
20 A. Leonidova, V. Pierroz, R. Rubbiani, J. Heier, S. Ferrari and G. Gasser, *Dalton Trans.*, 2014, **43**, 4287–4294.
21 A. Kastl, S. Dieckmann, K. Wähler, T. Völker, L. Kastl, A. L. Merkel, A. Vultur, B. Shannan, K. Harms, M. Ocker, W. J. Parak, M. Herlyn and E. Meggers, *ChemMedChem*, 2013, **8**, 924–927.
22 A. A. Abdel-Shafi, J. L. Bourdelande and S. S. Ali, *Dalton Trans.*, 2007, 2510–2516.
23 F. Ragone, H. H. Martinez Saavedra, P. M. David Gara, G. T. Ruiz and E. Wolcan, *J. Phys. Chem. A*, 2013, **117**, 4428–4435.
24 M. C. DeRosa and R. J. Crutchley, *Coord. Chem. Rev.*, 2002, **233–234**, 351–371.
25 S. Wang, R. Gao, F. Zhou and M. Selke, *J. Mater. Chem.*, 2004, **14**, 487–493.
26 R. R. Allison, H. C. Mota and C. H. Shibata, *Photodiagn. Photodyn. Ther.*, 2004, **1**, 263–277.
27 D. K. Chatterjee, L. S. Fong and Y. Zhang, *Adv. Drug Delivery Rev.*, 2008, **60**, 1627–1637.
28 J. P. Tardivo, A. D. Giglio, C. S. Oliveira, D. S. Gabrielli, H. C. Junqueira, D. B. Tada, D. Severino, R. F. Turchiello

and M. S. Baptista, *Photodiagn. Photodyn. Ther.*, 2005, **2**, 175–191.
29 K. Ishiyama, K. Nakamura, H. Ikai, T. Kanno, M. Kohno, K. Sasaki and Y. Niwano, *PLoS One*, 2012, **7**, e37871.
30 N. Wang, Z. Zhao, Y. Lv, H. Fan, H. Bai, H. Meng, Y. Long, T. Fu, X. Zhang and W. Tan, *Nano Res.*, 2014, **7**, 1291–1301.
31 J. C. Stockert, M. Canete, A. Juarranz, A. Villanueva, R. W. Horobin, J. I. Borrell, J. Teixido and S. Nonell, *Curr. Med. Chem.*, 2007, **14**, 997–1026.
32 O. Planas, T. Gallavardin and S. Nonell, *Chem. Commun.*, 2015, **51**, 5586–5589.
33 Y. You and W. Nam, *Chem. Soc. Rev.*, 2012, **41**, 7061–7084.
34 A. Kastl, A. Wilbuer, A. L. Merkel, L. Feng, P. Di Fazio, M. Ocker and E. Meggers, *Chem. Commun.*, 2012, **48**, 1863–1865.
35 S. Takizawa, R. Aboshi and S. Murata, *Photochem. Photobiol. Sci.*, 2011, **10**, 895–903.
36 C. Zhou and X. Zhao, *J. Organomet. Chem.*, 2011, **696**, 3322–3327.
37 W. Wu, P. Yang, L. Ma, J. Lalevée and J. Zhao, *Eur. J. Inorg. Chem.*, 2013, 228–231.
38 S. S. Lucky, K. C. Soo and Y. Zhang, *Chem. Rev.*, 2015, **115**, 1990–2042.
39 Y.-K. Peng, C.-W. Lai, C.-L. Liu, H.-C. Chen, Y.-H. Hsiao, W.-L. Liu, K.-C. Tang, Y. Chi, J.-K. Hsiao, K.-E. Lim, H.-E. Liao, J.-J. Shyue and P.-T. Chou, *ACS Nano*, 2011, **5**, 4177–4187.
40 C.-W. Lai, Y.-H. Wang, C.-H. Lai, M.-J. Yang, C.-Y. Chen, P.-T. Chou, C.-S. Chan, Y. Chi, Y.-C. Chen and J.-K. Hsiao, *Small*, 2008, **4**, 218–224.
41 J. Zhou, Q. Liu, W. Feng, Y. Sun and F. Li, *Chem. Rev.*, 2015, **115**, 395–465.
42 L. Gao, M. A. Peay and T. G. Gray, *Chem. Mater.*, 2010, **22**, 6240–6245.
43 (*a*) N. Lewinski, V. Colvin and R. Drezek, *Small*, 2008, **4**, 26–49; (*b*) F. Alexis, E. Pridgen, L. K. Molnar and O. C. Farokhzad, *Mol. Pharmacol.*, 2008, **5**, 505–515; (*c*) L. Sironi, S. Freddi, M. Caccia, P. Pozzi, L. Rossetti, P. Pallavicini, A. Dona, E. Cabrini, M. Gualtieri, I. Rivolta, A. Panariti, L. D'Alfonso, M. Collini and G. Chirico, *J. Phys. Chem. C*, 2012, **116**, 18407–18418; (*d*) P. Pallavicini, E. Cabrini, G. Cavallaro, G. Chirico, M. Collini, L. D'Alfonso, G. Dacarro, A. Donà, N. Marchesi, C. Milanese, A. Pascale, L. Sironi and A. Taglietti, *J. Inorg. Biochem.*, 2015, **151**, 123–131.
44 (*a*) K. Rahme, L. Chen, R. G. Hobbs, M. A. Morris, C. O'Driscoll and J. D. Holmes, *RSC Adv.*, 2013, **3**, 6085–6094; (*b*) H. Jans, K. Bonroy, R. De Palma, G. Reekmans, H. Jans, W. Laureyn, M. Smet, G. Borgh and M. Giido, *Langmuir*, 2008, **24**, 3949–3954.
45 (*a*) S. Schmidt, J. Nitschke and W. Trogler, *Inorg. Synth.*, 1989, **26**, 113–117; (*b*) D. Maggioni, F. Fenili, L. D'Alfonso, D. Donghi, M. Panigati, I. Zanoni, R. Marzi, A. Manfredi, P. Ferruti, G. D'Alfonso and E. Ranucci, *Inorg. Chem.*, 2012, **51**, 12776–12788.
46 P. Blondeau, M. Barboiu and E. Petit, *React. Funct. Polym.*, 2015, **86**, 259–263.
47 S. Benyahya, F. Monnier, M. Taillefer, M. Wong Chi Man, C. Bied and F. Ouazzani, *Adv. Synth. Catal.*, 2008, **350**, 2205–2208.
48 Rillema *et al.*[15b] obtained $[Re(L\text{-}L)(L')(CO)_3]^+$ complexes (where L–L is a bpy or a phen bidentate ligand, and L′ is a py like ligand) by a route that involves the tetracarbonyl intermediate $[Re(L\text{–}L)(CO)_4]OTf$, formed by stirring the precursor $Re(CO)_5OTf$ at room temperature in a non-coordinating solvent, in the presence of the bidentate ligand L–L. The $[Re(L\text{–}L)(L')(CO)_3]^+$ complex was subsequently obtained by the addition of one equiv. of the L′ ligand and refluxing for several hours. Another synthetic strategy proposed by Wrighton *et al.*[49] consisted in the substitution of the Cl^- ligand with a pyridine in the precursor $ReCl(CO)_3(L\text{–}L)$, by refluxing in the presence of AgOTf. We obtained the desired product by firstly preparing the precursor complex $[Re(phen)(CO)_3(OTf)]$ and then by easily substituting the OTf- anion with the py-upts ligand (Scheme 2).
49 S. M. Fredericks, J. C. Luong and M. S. Wrighton, *J. Am. Chem. Soc.*, 1979, **101**, 7415–7417.
50 J. Park, K. An, Y. Hwang, J.-G. Park, H.-J. Noh, J.-Y. Kim, J.-H. Park, N.-M. Hwang and T. Hyeon, *Nat. Mater.*, 2004, **3**, 891–895.
51 S. Santra, R. P. Bagwe, D. Dutta, J. T. Stanley, G. A. Walter, W. Tan and R. A. Mericle, *Adv. Mater.*, 2005, **17**, 2165–2169.
52 H. L. Ding, Y. X. Zhang, S. Wang, J. M. Xu, S. C. Xu and G. H. Li, *Chem. Mater.*, 2012, **24**, 4572–4580.
53 B. Radi, R. M. Wellard and G. A. George, *Soft Matter*, 2013, **9**, 3262–3271.
54 A. J. Kell, M. L. Barnes, Z. J. Jakubek and B. Simard, *J. Phys. Chem. C*, 2011, **115**, 18412–18421.
55 Also the IR spectra in the ν(CO) region indicate that the Re atom in the $[Re(phen)(CO)_3(py\text{-}upts)]^+$ complex is more electron rich than in the complex with unsubstituted pyridine (2034, 1934 cm^{-1}, *vs.* 2037, 1938 cm^{-1} for the complex with py ligand).
56 J. V. Caspar and T. J. Meyer, *J. Phys. Chem.*, 1983, **87**, 952–957.
57 M. Wrighton and D. L. Morse, *J. Am. Chem. Soc.*, 1974, **96**, 998–1003.
58 G. Ferrante and S. Sykora, *Adv. Inorg. Chem.*, 2005, **57**, 405–470.
59 see for instance ref.: (*a*) V. Amendola, M. Meneghetti, O. M. Bakr, P. Riello, S. Polizzi, S. Fiameni, D. H. Anjum, P. Arosio, T. Orlando, C. de Julian Fernandez, F. Pineider, C. Sangregorio and A. Lascialfari, *Nanoscale*, 2013, **5**, 5611–5619; (*b*) W. Di, S. K. P. Velu, A. Lascialfari, C. Liu, N. Pinna, P. Arosio, Y. Sakka and W. Qin, *J. Mater. Chem.*, 2012, **22**, 20641–20648; (*c*) H. Amiri, R. Bustamante, A. Millán, N. J. O. Silva, R. Piñol, L. Gabilondo, F. Palacio, P. Arosio, M. Corti and A. Lascialfari, *Magn. Reson. Med.*, 2011, **66**, 1715–1721.
60 W. Wu, P. Yang, L. Ma, J. Lalevée and J. Zhao, *Eur. J. Inorg. Chem.*, 2013, 228–231.
61 D. Maggioni, M. Galli, L. D'Alfonso, D. Inverso, M. V. Dozzi, L. Sironi, M. Iannacone, M. Collini, P. Ferruti, E. Ranucci and G. D'Alfonso, *Inorg. Chem.*, 2015, **54**, 544–553.

62 C. Tanielian and C. Wolff, *J. Phys. Chem.*, 1995, **99**, 9831–9837.
63 S. J. Leach and H. A. Scher, *J. Am. Chem. Soc.*, 1960, **82**, 4790–4792.
64 W. Tang, H. Xu, R. Kopelman and M. A. Philbert, *Photochem. Photobiol.*, 2005, **81**, 242–249 and refs therein.
65 The much higher yields reported for some Re complexes[20,66] were measured in organic apolar solvents, where non-radiative deactivation pathways of the excited states are less available.
66 Z. Yi, J. Zhao, J. Sun, S. Guo and H. Zhang, *Dalton Trans.*, 2013, **42**, 2062–2074.
67 D. B. Tada, L. L. R. Vono, E. L. Duarte, R. Itri, P. K. Kiyohara, M. S. Baptista and L. M. Rossi, *Langmuir*, 2007, **23**, 8194–8199.
68 W. Denk, J. Strickler and W. Webb, *Science*, 1990, **248**, 73–76.
69 N. L. Oleinick, R. L. Morris and I. Belichenko, *Photochem. Photobiol. Sci.*, 2002, **1**, 1–21.